A Black-Oil Model for Primary and Secondary Oil-Recovery in Stratified Petroleum Reservoirs

A. Dollari*, Ch. Chatzichristos and A. G. Yiotis
Environmental Research Laboratory, National Center for Scientific Research "Demokritos", 15341 Athens, Greece
*Corresponding author: natasa@ipta.demokritos.gr

Abstract: The black-oil model is a multiphase fluid flow formulation extensively used in the petroleum recovery industry for the prediction of oil/gas recovery rates and the evolution of petroleum reservoir conditions. In this contribution, we propose a numerically stable formulation of the black-oil model with negligible capillary pressure. The formulation is based on the oil phase pressure and total fluid velocity and solved numerically using the PDE interface of COMSOL Multiphysics in the general and coefficient mode for time-dependent analysis. We apply the proposed model in a series of typical primary and secondary oil recovery processes ranging from the natural pressure-driven fluid expansion and solution-gas drive during the early-life of the reservoir to more elaborate pressure maintenance strategies relying on waterflooding and gas injection in a typical homogeneous petroleum reservoir.

Keywords: black-oil model, porous media, petroleum reservoir, solution-gas drive, secondary oil-recovery

1. Introduction

Black-oil simulators are commonly used in petroleum reservoir engineering for the prediction of oil production dynamics, especially during the earlier stages of oil-field exploitation, while also serving to guide pressure maintenance strategies in the longer term. The main assumption of such an approach (as opposed to compositional flow models) is the classification of all reservoir species into two main categories with respect to their physical state at surface conditions; 1. A mixture of heavy H/C components containing all species that exist in a liquid form at the surface (denoted as "o"), and 2. A mixture of volatile H/C components that contain all species that exist as a gaseous phase at surface conditions (denoted as "g"). Furthermore, the aqueous phase (w), which is abundant in petroleum reservoirs, is considered as the third flowing phase [1, 2].

The apparent densities of the above fluid phases are expressed as functions of appropriate experimentally-determined fluid formation volume factors and solution ratios to implement the effects of fluid compressibility, phase change and species dissolution across the volatile and heavy H/C mixtures at elevated reservoir pressures (Pressure-Volume-Temperature, PVT tables). The resulting multiphase flow problem is then treated using a phenomenological generalization of Darcy's law, where the relative permeability of each fluid through the porous structure is expressed as a state function of local saturation.

2. Theory/ Governing Equations

The black-oil model relies on the coupled solution of mass conservation equations for the water (w), oil (o) and gas (g) phases (or mixtures) subject to appropriate boundary and initial conditions, while also accounting for mass transfer of dissolved species across the (o) and (g) phases. The basic partial differential equations for the black-oil model in a porous medium expressed as a conservation of the mass of the volatile species, the heavy species and water reads as follows [3, 4];

$$\phi \frac{\partial}{\partial t}\left(\frac{S_g}{B_g}+\frac{R_{so}S_o}{B_o}\right)+\nabla\cdot\left(\frac{1}{B_g}\boldsymbol{u_g}+\frac{R_{so}}{B_o}\boldsymbol{u_o}\right)=q_g, \quad (1)$$

$$\phi \frac{\partial}{\partial t}\left(\frac{S_o}{B_o}\right)+\nabla\cdot\left(\frac{1}{B_o}\boldsymbol{u_o}\right)=q_o, \quad (2)$$

$$\phi \frac{\partial}{\partial t}\left(\frac{S_w}{B_w}\right)+\nabla\cdot\left(\frac{1}{B_w}\boldsymbol{u_w}\right)=q_w \quad (3)$$

where the volumetric phase velocity is given by

$$\boldsymbol{u_\alpha}=-\frac{k_{r\alpha}}{\mu_\alpha}\boldsymbol{K}\left(\nabla p_\alpha-\rho_\alpha \boldsymbol{g}\right);\quad \alpha = g, o, w \quad (4)$$

Here ϕ and $\boldsymbol{K}$ denote the porosity and intrinsic permeability tensor of the porous medium, $S_\alpha, \mu_\alpha, \rho_\alpha, p_\alpha, \boldsymbol{u_\alpha}, B_\alpha, k_{r\alpha}$ and q_α the α -phase saturation, viscosity, density, pressure, volumetric velocity, formation volume factor,

relative permeability, and external source term, respectively. R_{so} is the gas solubility in the oil phase and $\boldsymbol{g}$ is the acceleration of gravity.

The system is closed by the local constraints. The three phases jointly fill up the void space:

$$S_g + S_o + S_w = 1 \quad (5)$$

while the phase pressures p_g, p_o, p_w are related by gas-oil and and oil-water capillary pressures, respectively:

$$p_{cgo} = p_g - p_o, \quad p_{cow} = p_o - p_w \quad (6)$$

It is also assumed that the porous media is fully saturated but the phases are separated at the pore-scale, the porous matrix and fluids are slightly compressible, diffusion is neglected for all phases and the whole system is in local thermodynamic equilibrium [2, 5, 6].

3. Numerical Model

The black-oil model is typically solved numerically with finite volumes or finite differences approaches [1]. The discretization under the finite element framework utilized by COMSOL requires that the non-linearity and coupling among the equations are weakened, while preserving the main physical properties and constraints. Thus a more appropriate, numerically stable, reformulation of the governing equations is developed, which is based on the oil phase pressure and total fluid velocity as proposed by Chen [2].

3.1 Phase Formulation based on Oil Pressure and Total Velocity

For a better demonstration of the adopted formulation, we first introduce the phase mobility functions $\lambda_\alpha = k_{r\alpha}/\mu_\alpha$ for $\alpha = g, o, w$, and the total mobility $\lambda = \sum \lambda_\alpha$. We also define the fractional flow functions $f_\alpha = \lambda_\alpha/\lambda$, so that $\sum f_\alpha = 1$.

Oil being a continuous phase implies that p_o is well behaved, so we use the oil phase pressure as the pressure variable:

$$p = p_o \quad (7)$$

We now define the total velocity:

$$\boldsymbol{u} = \sum \boldsymbol{u}_\alpha \quad (8)$$

Then we perform the corresponding notation substitution and we use Eqs. (7) and (8), carry out the differentiation indicated in Eqs. (1) – (3) and apply Eqs. (4) – (6) to obtain the differential equations:

Pressure equation

$$\nabla\cdot\boldsymbol{u} = \sum_{\beta=g,o,w} B_\beta\left(q_\beta - \phi S_\beta \frac{\partial}{\partial t}\left(\frac{1}{B_\beta}\right) - \boldsymbol{u}_\beta\cdot\nabla\left(\frac{1}{B_\beta}\right)\right) - B_g\left(R_{so}q_o + \frac{\phi S_o}{B_o}\frac{\partial R_{so}}{\partial t} + \frac{1}{B_o}\boldsymbol{u}_o\cdot\nabla R_{so}\right), \quad (9)$$

$$\boldsymbol{u} = -\boldsymbol{K}\lambda\left(\nabla p - G_\lambda + \sum_\beta f_\beta \nabla p_{c\beta o}\right)$$

Saturation equations

$$\phi\frac{\partial S_\alpha}{\partial t} + \nabla\cdot\boldsymbol{u}_\alpha = B_\alpha\left(q_\alpha - \phi S_\alpha\frac{\partial}{\partial t}\left(\frac{1}{B_\alpha}\right) - \boldsymbol{u}_\alpha\cdot\nabla\left(\frac{1}{B_\alpha}\right)\right), \quad (10)$$

$$\boldsymbol{u}_\alpha = f_\alpha\boldsymbol{u} + \boldsymbol{K}f_\alpha\sum_\beta \lambda_\beta\left(\nabla\left(p_{c\beta o} - p_{c\alpha o}\right) - \left(\rho_\beta - \rho_\alpha\right)\boldsymbol{g}\right)$$

for $\alpha = o, w$, where

$$G_\lambda = \boldsymbol{g}\sum_\beta f_\beta\rho_\beta \quad (11)$$

3.2 Numerical Implementation in COMSOL

The numerical model of Eqs. (9)-(10) is implemented in COMSOL 5.3 using the PDE Interface in the general and coefficient form for time dependent analysis [7]. The General Form PDE (g) is used for Eq. 9 with the total phase pressure, p, as the dependent variable. For completeness we provide below the exact user-defined expressions for the built-in variables used (maintaining COMSOL's naming convention):

$$e_a = 0, \quad d_a = 0, \quad \boldsymbol{\Gamma} = \begin{bmatrix} u_{ox} \\ u_{oy} \end{bmatrix},$$

$$f = -B_g\left(-q_g + \phi S_g\frac{\partial}{\partial t}\left(\frac{1}{B_g}\right) + u_{gx}\frac{\partial}{\partial x}\left(\frac{1}{B_g}\right) + u_{gy}\frac{\partial}{\partial y}\left(\frac{1}{B_g}\right)\right) - B_o\left(-q_o + \phi S_o\frac{\partial}{\partial t}\left(\frac{1}{B_o}\right) + u_{ox}\frac{\partial}{\partial x}\left(\frac{1}{B_o}\right) + u_{oy}\frac{\partial}{\partial y}\left(\frac{1}{B_o}\right)\right) - B_w\left(-q_w + \phi S_w\frac{\partial}{\partial t}\left(\frac{1}{B_w}\right) + u_{wx}\frac{\partial}{\partial x}\left(\frac{1}{B_w}\right) + u_{wy}\frac{\partial}{\partial y}\left(\frac{1}{B_w}\right)\right) - B_g\left(-q_o R_{so} + \frac{\phi S_o}{B_o}\frac{\partial R_{so}}{\partial t} + \frac{1}{B_o}\left(u_{ox}\frac{\partial R_{so}}{\partial x} + u_{oy}\frac{\partial R_{so}}{\partial y}\right)\right)$$

The Coefficient Form PDE (c) is used for Eq. 10 with S_o and S_w as the dependent variables (i.e. two equations for oil and water saturation, respectively).

The exact user-defined expressions for the oil phase saturation read;

$$e_a=0,\ \ d_a=\phi,\ \ c=\varepsilon,\ \ a=0,$$
$$\boldsymbol{\beta}=\begin{bmatrix}0\\0\end{bmatrix},\ \ \boldsymbol{\alpha}=\begin{bmatrix}0\\0\end{bmatrix},\ \ \boldsymbol{\gamma}=\begin{bmatrix}u_{ox}\\u_{oy}\end{bmatrix},$$
$$f=-B_o\left(\phi S_o\frac{\partial}{\partial t}\left(\frac{1}{B_o}\right)+u_{ox}\frac{\partial}{\partial x}\left(\frac{1}{B_o}\right)+u_{oy}\frac{\partial}{\partial y}\left(\frac{1}{B_o}\right)\right)$$

while for the water saturation we write;

$$e_a=0,\ \ d_a=\phi,\ \ c=\varepsilon,\ \ a=0,$$
$$\boldsymbol{\beta}=\begin{bmatrix}0\\0\end{bmatrix},\ \ \boldsymbol{\alpha}=\begin{bmatrix}0\\0\end{bmatrix},\ \ \boldsymbol{\gamma}=\begin{bmatrix}u_{wx}\\u_{wy}\end{bmatrix},$$
$$f=-B_w\left(\phi S_w\frac{\partial}{\partial t}\left(\frac{1}{B_w}\right)+u_{wx}\frac{\partial}{\partial x}\left(\frac{1}{B_w}\right)+u_{wy}\frac{\partial}{\partial y}\left(\frac{1}{B_w}\right)\right)$$

Given that capillary forces among the three fluid components are neglected, the total and individual phase velocities can be rewritten as follows;

$$\begin{aligned}\boldsymbol{u}&=-\boldsymbol{K}\lambda\left(\nabla p-\boldsymbol{g}\left(f_g\rho_g+f_o\rho_o+f_w\rho_w\right)\right),\\ \boldsymbol{u_g}&=f_g\boldsymbol{u}-\boldsymbol{K}\,\mathrm{f}_g\left(\lambda_o\left(\rho_o-\rho_g\right)+\lambda_w\left(\rho_w-\rho_g\right)\right)\boldsymbol{g},\\ \boldsymbol{u_o}&=f_o\boldsymbol{u}-\boldsymbol{K}\,\mathrm{f}_o\left(\lambda_g\left(\rho_g-\rho_o\right)+\lambda_w\left(\rho_w-\rho_o\right)\right)\boldsymbol{g},\\ \boldsymbol{u_w}&=f_w\boldsymbol{u}-\boldsymbol{K}\,\mathrm{f}_w\left(\lambda_g\left(\rho_g-\rho_w\right)+\lambda_o\left(\rho_o-\rho_w\right)\right)\boldsymbol{g}\end{aligned}\qquad(12)$$

Finally, the phase densities at reservoir conditions are expressed as follows;

$$\rho_o=\frac{\rho_{Os}+R_{so}\rho_{Gs}}{B_o},\ \ \rho_g=\frac{\rho_{Gs}}{B_g},\ \ \rho_w=\frac{\rho_{Ws}}{B_w}\qquad(13)$$

where the underscript "s" designates properties at standard (surface) conditions.

In the Appendix, we provide the complete set of values for phase densities at standard conditions, the PVT phase properties as well as the two-phase relative permeability curves for the gas-oil and the oil-water system. In the following simulations water and the solid phase are assumed practically incompressible.

4. Numerical Simulations / Results

We consider an inclined homogeneous, but anisotropic, petroleum reservoir, with a typical porosity of φ=0.2, that exhibits a series of structural traps as shown in Figure 1. The structure is overlaid by an impermeable caprock that imposes the trapping of petroleum and the subsequent formation of the reservoir in the geological time-scale.

We assume that the reservoir is characterized by an anisotropic permeability tensor where the longitudinal component follows the direction of the lower reservoir boundary, while the transverse component is always normal to that. Given that a fixed Cartesian coordinate system is used to express the gradients of pressure that control flow in the x and y-directions, the permeability tensor needs to account for the direction of the longitudinal permeability (that coincides with the bottom boundary of the reservoir) with respect to the x-axis. This effect is parametrized by the angle θ between the two vectors as shown also in Figure 1. In this domain the angle obeys the expression $\theta=atan(-0.297x+1.125)[rad]$ and this effect generates a permeability tensor with no-zero off-diagonal terms in the x-y Cartesian system, as shown below;

$$\boldsymbol{K}=\begin{bmatrix}k_{max}\cos^2\theta+k_T\sin^2\theta & k_{max}\cos\theta\sin\theta-k_T\cos\theta\sin\theta\\ k_{max}\sin\theta\cos\theta-k_T\sin\theta\cos\theta & k_{max}\sin^2\theta+k_T\cos^2\theta\end{bmatrix}$$
$$=\begin{bmatrix}k_{11} & k_{12}\\ k_{21} & k_{22}\end{bmatrix}$$

Darcy's equation in the x,y-directions is then expressed as follows for the α -phases;

$$\begin{aligned}&\boldsymbol{u_\alpha}=(u_{\alpha x},u_{\alpha y}),\\ &u_{\alpha x}=-\lambda_\alpha(k_{11}(\partial p/\partial x)+k_{12}((\partial p/\partial y)+\rho_\alpha g_y))\\ &u_{\alpha y}=-\lambda_\alpha(k_{21}(\partial p/\partial x)+k_{22}((\partial p/\partial y)+\rho_\alpha g_y))\end{aligned}$$

Initially the two phases are distributed equally in the pore space with an initial average oil phase saturation of 90% PV, as shown in the next 2-D surface plot.

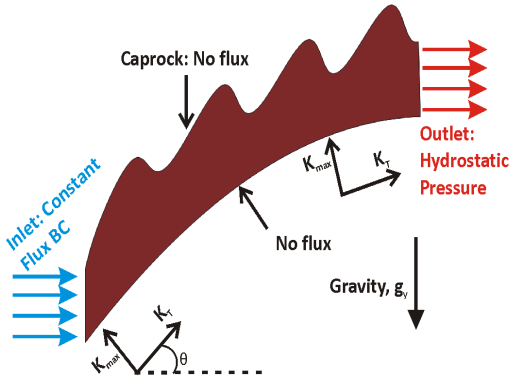

Figure 1. Schematic of the down-scaled petroleum reservoir used in our numerical simulations exhibiting a series of structural traps on the top boundary below an impermeable caprock (not shown here). The longitudinal permeability component follows the direction of the bottom boundary of the reservoir.

The initial reservoir pressure is taken assuming hydrostatic conditions at a depth where the oil phase is under-saturated (above the bubble point in the phase envelope). The fluids are then allowed to escape from the formation

from a production well located along the right boundary.

In the following section, we employ the previously described black-oil model to solve a series of typical oil production scenarios, including oil production due to the natural initial pressure of the formation and the pressure depletion that allows for solution-gas drive, and secondary oil recovery scenarios, including waterflooding.

Initial conditions

$$p(t_0) = p_{in} = 10^5 + \rho_w g(2860 - y)\,[Pa]$$
$$S_o(t_0) = 1 - S_{wc}$$
$$S_w(t_0) = S_{wc} = 0.1$$

No flux conditions are applied in the side walls and no external source terms are considered.

4.1 Primary Oil-recovery: Solution-gas Drive Mechanism

The flow of oil and gas phases through porous media during a primary recovery process driven by the liberation of the dissolved gas component is simulated. A smooth pressure drop-down is applied for a time period of 12000s at the right boundary.

Table 1: Primary recovery simulation data

Property	Unit	Value
Maximum permeability (k_{max})	m^2	10^{-12}
Transverse permeability (k_T)	m^2	10^{-13}
Numerical diffusion (ε)	m^2/s	10^{-7}

Boundary conditions

Outlet

$p = p_{out}$

$$-\boldsymbol{n}\cdot(-\varepsilon\nabla S_o + \boldsymbol{u}_o) = -\boldsymbol{u}_o$$
$$-\boldsymbol{n}\cdot(-\varepsilon\nabla S_w + \boldsymbol{u}_w) = -\boldsymbol{u}_w$$
$$where\ p_{out} = p_{in} - 0.2\cdot p_{in}\cdot flc2hs(t - t_1, t_2)\,[Pa]$$
$$for\ t_1 = 7000\,s, t_2 = 6800\,s$$

The oil phase saturation evolution and the fluid productions at surface conditions are presented.

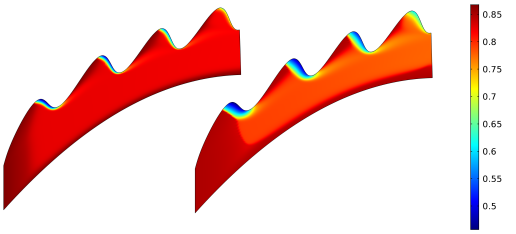

Figure 2. Oil phase saturation during primary oil-recovery for t = 8000s (left) and t = 12000s (right).

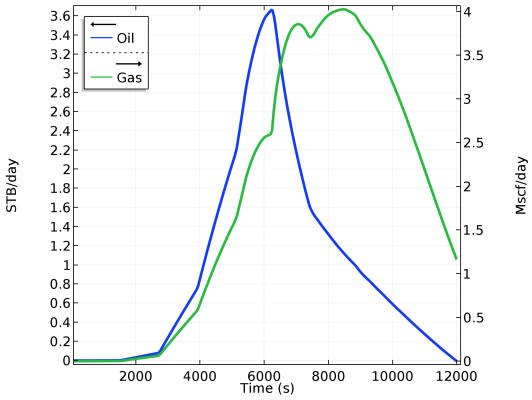

Figure 3. Fluid production rates at standard conditions during primary oil-recovery.

During the initial stages only the oil component and the dissolved gas component are produced since the petroleum reservoir is still under-saturated. As the average reservoir pressure declines, gas is generated causing a phase segregation due to gravitational forces. From that point and on the oil follows a decaying rate till the end of simulation study. Similarly, the gas production follows an increasing rate and then declines smoothly.

4.2 Secondary Oil-recovery

The next problems simulate the flow behavior during waterflooding and gas injection processes in petroleum reservoirs. Although normally the fluids are injected only from the upper or bottom part of the injection well respectively for better sweep efficiency, in the current studies they are injected from the whole side of the left boundary of the domain for demonstration purposes. Accordingly, the production well is placed in the right boundary.

4.2.1 Waterflooding

The simulation of a waterflooding process in an anisotropic reservoir is studied. The water is injected for 10000s.

Boundary conditions

Inlet	Outlet
$-\boldsymbol{n}\cdot\boldsymbol{u}=u_{\text{in}}$	$p=p_{out}=p_{\text{in}}$
$S_o=S_{\text{or}}$	$-\boldsymbol{n}\cdot(-\varepsilon\nabla S_o+\boldsymbol{u_o})=-\boldsymbol{u_o}$
$S_w=1-S_{\text{or}}$	$-\boldsymbol{n}\cdot(-\varepsilon\nabla S_w+\boldsymbol{u_w})=-\boldsymbol{u_w}$

Table 2: Waterflooding simulation data

Property	Unit	Value
Maximum permeability (k_{max})	m^2	$5\ 10^{-11}$
Transverse permeability (k_T)	m^2	$5\ 10^{-12}$
Oil residual saturation (S_{or})	-	0.3
Inlet velocity (u_{in})	m/s	10^{-4}
Numerical dispersion (ε)	m^2/s	$5\ 10^{-6}$

The evolution of the oil phase saturation during the water-injection and the fluid productions at surface conditions are presented.

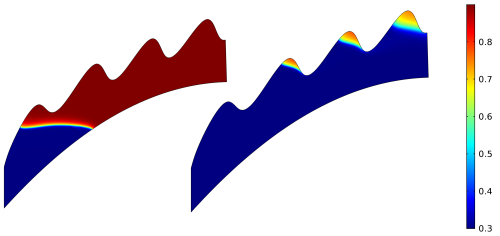

Figure 4. Oil phase saturation during waterflooding for t = 1500s (left) and t = 10000s (right)

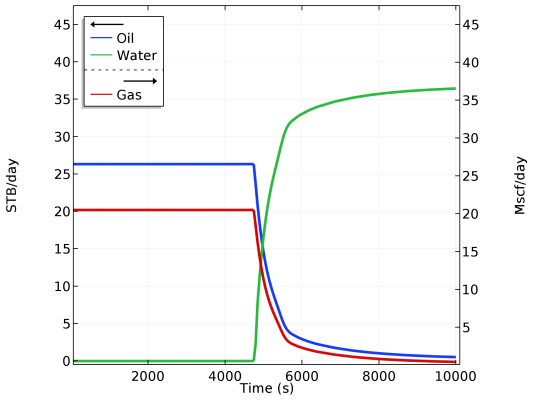

Figure 5. Fluid production rates at standard conditions during waterflooding.

As water floods enter the reservoir, the saturation of the oil phase gradually decreases in the area near the injector leading to a larger swept zone with time. During this time period the oil is produced with constant rate, followed by an abrupt decrease which is indicative of the water breakthrough. The two rates exhibit then a reverse proportional relationship till the end of the simulation study, when the efficient sweeping is visually verified.

4.2.2 Gas Injection

The simulation of a gas injection process in an isotropic reservoir is studied. The gas is injected for a time period of 45000 s.

Boundary conditions

Inlet	Outlet
$-\boldsymbol{n}\cdot\boldsymbol{u}=u_{\text{in}}$	$p=p_{out}=p_{\text{in}}$
$S_o=S_{\text{or}}$	$-\boldsymbol{n}\cdot(-\varepsilon\nabla S_o+\boldsymbol{u_o})=-\boldsymbol{u_o}$
$S_w=S_{\text{wc}}$	$S_w=S_{\text{wc}}$

Table 3: Gas injection simulation data

Property	Unit	Value
Isotropic permeability ($k_{iso} = k_{max} = k_T$)	m^2	10^{-12}
Inlet velocity (u_{in})	m/s	10^{-5}
Numerical diffusion (ε)	m^2/s	$8\ 10^{-7}$

Following are the evolution of the oil phase saturation during the gas injection and the production rates at surface conditions.

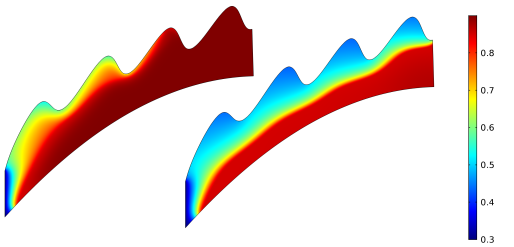

Figure 6. Oil phase saturation during gas injection for t = 4860s (left) and 45000s (right).

The lighter gas floods travel quickly to the upper part of the reservoir due to buoyancy, thus displacing non-uniformly the oil phase towards the production well. The oil recovery exhibits a constant rate till the gas breakthrough, which causes a smooth reduction till the end of the simulation study. Gas is produced at surface conditions with a constant rate from the beginning of the injection as it exists initially as solution in the oil phase in reservoir conditions. The abrupt increase indicates that the gas floods have reached the production well, thus they are

recovered together with the oil phase until the end of the injection process.

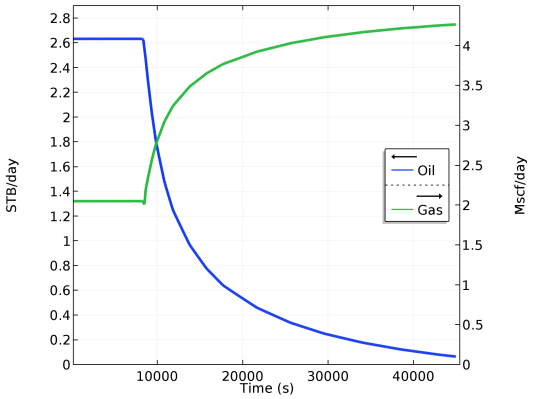

Figure 7. Fluid production rates at standard conditions during gas injection.

By the end, the gas phase has occupied the upper part of the reservoir, leaving however a significant volume of oil in the half bottom part. The sweeping efficiency is clearly smaller in the current case, due to the formation of an upper preferable gas path by the time of the breakthrough.

5. Conclusions

In this contribution we propose a black-oil model using COMSOL's PDE Interface based on the oil phase pressure and total fluid velocity formulation developed by Chen [2]. Our implementation is then evaluated for an homogeneous petroleum reservoir exhibiting a series of structural traps for typical primary and secondary oil recovery processes, including initial pressure depletion (solution gas-drive mechanism), waterflooding and gas injection.

The interpretation of the physical phenomenon is described successfully enough by the implemented numerical model. The water/gas injection which is significantly enhanced due to buoyancy that leads to accumulation of injected water/gas in the bottom/upper part of the reservoir thus pushing the lighter/heavier oil towards the surface and production wells is visually verified via 2-D plots. Apparent is also the phase segregation in the reservoir by the end of the pressure depletion, as expected.

The newly-developed numerical model can hence be used as an independent PDE-module in reservoir simulation studies but also for more complex problems in Enhanced Oil Recovery (EOR) processes by implementing also the appropriate PDEs that describe tracer (mass) transfer, thermal stimulation and surfactant processes.

6. References

1. Z Chen, G Huan, and Y Ma, *Computational Methods for Multiphase Flows in Porous Media*, Computational Science and Engineering. Society for Industrial and Applied Mathematics (2006)
2. Z Chen, *Formulations and Numerical Methods of the Black Oil Model in Porous Media*, Society for Industrial and Applied Mathematics, **38**, 489-514 (2000)
3. K Aziz and A Settari, *Petroleum Reservoir Simulation*. Applied Science Publishers Ltd., London UK (1979)
4. D W Peaceman, *Fundamentals of numerical reservoir simulation*. Elsevier, New York (1977)
5. J Bear, *Dynamics of Fluids in Porous Media*. Dover Civil and Mechanical Engineering Series, Dover (1972)
6. M A Diaz-Viera, D A Lopez-Falcon, A Moctezuma-Berthier, and A Ortiz-Tapia, *COMSOL implementation of a multiphase fluid flow model in porous media*, COMSOL Conference, Boston (2008)
7. COMSOL Mutliphysics Reference Manual, Version 5.3", COMSOL, Inc. (2017)

7. Appendix

Table 4: Fluid densities at standard conditions

Fluid	Density at SC (kg/m^3)
Gas	0.40
Oil	800
Water	1000

Table 5: Oil phase properties

Pressure (MPa)	R_{so} (sm^3/sm^3)	B_o (vol/svol)	μ_o (cP)
8.38	24.4	1.172	1.970
9.75	34.7	1.200	1.556
11.1	42.9	1.221	1.397
12.5	51.3	1.242	1.280
15.3	66.8	1.278	1.095
18.0	82.2	1.320	0.967
20.8	99.4	1.360	0.848
23.5	117.7	1.402	0.762
26.3	137.1	1.447	0.691
29.1	137.1	1.4405	0.694
31.8	137.1	1.434	0.697

Table 6: Gas phase properties

Pressure (MPa)	B_g (vol/svol)	μ_g (cP)
8.38	0.0783	0.0124
9.75	0.0395	0.0125
11.1	0.0261	0.0128
12.5	0.0194	0.0130
15.3	0.0126	0.0139
18.0	0.0092	0.0148
20.8	0.0072	0.0161
23.5	0.0059	0.0173
26.3	0.0050	0.0187

Table 7: Water phase properties

Pressure (MPa)	B_w (vol/svol)	μ_w (cP)
27.52	1.0231	0.94

Table 8: Water and gas phase relative permeabilities

S_w	kr_w	S_g	kr_g
0.1	0.0	0	0
0.16	0.0005	0.05	0
0.22	0.004	0.09	0.032
0.28	0.0135	0.18	0.089
0.34	0.032	0.27	0.164
0.40	0.0625	0.36	0.253
0.46	0.108	0.45	0.354
0.52	0.172	0.54	0.465
0.58	0.256	0.63	0.586
0.64	0.365	0.72	0.716
0.70	0.50	0.81	0.854
0.80	0.667	0.9	1
0.90	0.833		
1	1		

Table 9: Oil phase relative permeabilities

S_o	kr_o (water-oil system)	kr_o (gas-oil system)
0.3	0.0	0
0.36	0.032	0.001
0.42	0.089	0.008
0.48	0.164	0.0275
0.54	0.253	0.064
0.60	0.354	0.125
0.66	0.465	0.216
0.72	0.586	0.343
0.78	0.716	0.512
0.84	0.854	0.729
0.90	1	1